Publication Year	2022
Acceptance in OA	2022-03-23T16:05:17Z
Title	The Coaxial L-P Cryogenic Receiver of the Sardinia Radio Telescope
Authors	VALENTE, Giuseppe, PISANU, Tonino, NAVARRINI, Alessandro, MARONGIU, Pasqualino, ORFEI, ALESSANDRO, MARIOTTI, SERGIO, NESTI, Renzo, RODA, JURI, CATTANI, ALESSANDRO, BOLLI, Pietro, MONTISCI, GIORGIO
Publisher's version (DOI)	10.1109/ACCESS.2021.3139744
Handle	http://hdl.handle.net/20.500.12386/31826
Journal	IEEE ACCESS
Volume	10

IEEE Access
Multidisciplinary : Rapid Review : Open Access Journal

Received December 4, 2021, accepted December 29, 2021, date of publication December 30, 2021,
date of current version January 7, 2022.

Digital Object Identifier 10.1109/ACCESS.2021.3139744

The Coaxial L-P Cryogenic Receiver of the Sardinia Radio Telescope

GIUSEPPE VALENTE[1], TONINO PISANU[2], ALESSANDRO NAVARRINI[2], PASQUALINO MARONGIU[2], ALESSANDRO ORFEI[3], SERGIO MARIOTTI[3], RENZO NESTI[4], JURI RODA[3], ALESSANDRO CATTANI[3], PIETRO BOLLI[4], AND GIORGIO MONTISCI[2,5], (Senior Member, IEEE)
[1]Italian Space Agency (ASI), 00133 Rome, Italy
[2]INAF-Osservatorio Astronomico di Cagliari, 09047 Selargius, Italy
[3]INAF-Istituto di Radioastronomia, 40127 Bologna, Italy
[4]INAF-Osservatorio Astrofisico di Arcetri, 50125 Firenze, Italy
[5]Dipartimento di Ingegneria Elettrica ed Elettronica, Università degli Studi di Cagliari, 09123 Cagliari, Italy

Corresponding authors: Tonino Pisanu (tonino.pisanu@inaf.it) and Giorgio Montisci (giorgio.montisci@unica.it)

ABSTRACT The design and characterization of the coaxial dual-band L-P radio astronomical receiver for the prime focus of the Sardinia radio telescope are presented. The main feature of this receiver is to allow simultaneous radio astronomical observations in the P (305 – 410 MHz) and L (1.3 – 1.8 GHz) frequency bands. This functionality, which has been requested by the Pulsar research group at the National Institute for Astrophysics to estimate, among the others, the ionospheric dispersion in Pulsar observation, is currently missing in any other radio astronomical facility throughout the world. Also, single band operation is ensured by the proposed design both in linear and circular polarization, making this L-P receiver an ideal instrument for a wide range of radio astronomical and space applications. Some components of the receiver chain have been housed inside a cryostat and refrigerated at 20 K to reduce the noise temperature, resulting in a good performance compared to the receivers of other large radio telescopes. Several challenging issues have been faced in the design, mainly due to the large dimension and weight of the overall structure to be mounted in the prime focus position. Moreover, the design of the cryostat was constrained by the limited space available in the direction of the optical axis inside the focal cabin of the radio telescope, requiring a compact and light realization of the components of the receiver chain. This called for a home-made design of several devices, requiring a strong collaborative effort by researchers, engineers, and astronomers.

INDEX TERMS Antennas, radio astronomy, receivers, reflector antennas.

I. INTRODUCTION

The Sardinia Radio Telescope (SRT) is a general-purpose fully steerable 64-meter diameter radio telescope designed to operate with high efficiency across the 0.3-116 GHz frequency range [1]–[4]. The radio observatory is the result of the scientific and technical collaboration among three separate organizations of the Italian National Institute for Astrophysics (INAF): the Institute of Radio Astronomy (IRA), the Cagliari Astronomical Observatory (OAC), and the Arcetri Astrophysical Observatory (OAA). The main funding agencies are the Italian Ministry of Education, University and Research (MIUR), the Sardinia Regional Government (RAS), the Italian Space Agency (ASI), and INAF itself. The SRT is designed to be used for astronomy, geodesy, and space science, both as a single dish and as part of European and International Very Large Baseline Interferometry (VLBI) networks. The SRT operates as an international facility, with regular worldwide distributed calls for proposal, and no a priori limitation based on the affiliation of the proposers. A large fraction of the observing time (of the order of 80%) is devoted to radio astronomy applications, while 20% of the time is allocated to activities of interest to ASI, i.e. space applications and the follow-up of space science missions [5]. Recently, the telescope has also been used for Space Surveillance and Tracking (SST) [6]–[8].

The telescope is located 35 km North of Cagliari (Italy) at about 600 m above the sea level. To minimize spillover and

The associate editor coordinating the review of this manuscript and approving it for publication was Yiming Huo.

standing waves, the SRT optical design is based on a quasi-Gregorian configuration (Fig. 1) with a shaped 64-meter diameter primary reflector (M1) and a 7.9-meter diameter secondary reflector (M2). The primary reflector is equipped with an active surface, consisting of 1008 aluminum panels (with a panel manufacturing root-mean-square error (RMSE) less than 70 μm) and of 1116 electromechanical actuators able to compensate the gravitational deformation of the backup structure. The primary reflector has been aligned with a RMSE of 290 μm using photogrammetry. Currently, the metrology system is being upgraded to improve the RMSE to a level of 150 μm and enable high antenna efficiency observations up to the 3 mm band (with 116 GHz maximum frequency).

SRT has been designed to host up to twenty receivers, which can be installed in six different focal positions:

i. Primary focus (F1) with focal length to diameter ratio (F/D) equal to 0.33, ideal for receivers operating in the frequency range 0.3 GHz – 20 GHz.
ii. Gregorian focus (F2) with F/D equal to 2.34, frequency range 7.5 GHz - 116 GHz.
iii. Beam-wave guide foci (F3&F4 and F5&F6) with F/D 1.38 and 2.81, respectively, frequency range 1.4 GHz - 35 GHz.

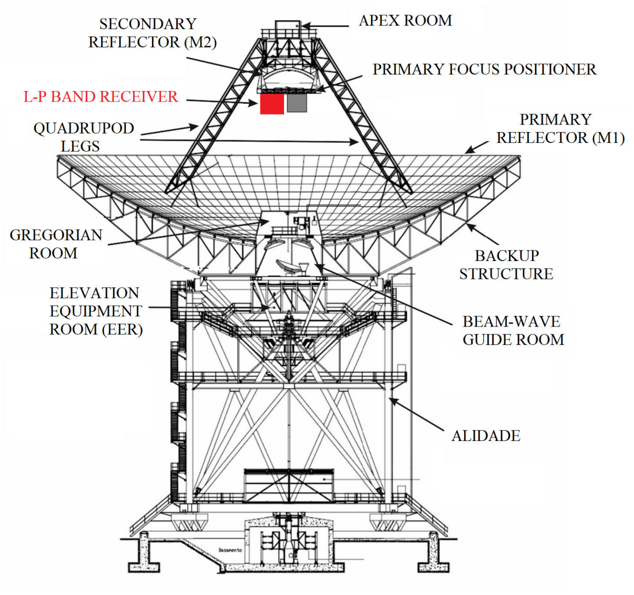

FIGURE 1. Sketch of the Sardinia Radio Telescope.

In this work we will describe the development, design, and realization of the cryogenic coaxial dual-frequency L-P band receiver of the SRT, which has been installed on the primary focus (F1) of the antenna and allows concurrent observations in the P and L frequency bands, as well as observations in a single band (either P-band or L-band). This receiver operates in both linear and circular polarization, allowing observation of a wide range of radio astronomical phenomena.

Among the largest radio telescopes in the world (see table 1), to the best knowledge of the authors the SRT is the only one equipped with a dual-frequency receiver that covers the P and L frequency bands (Fig. 2), and this makes it the ideal instrument for several radio astronomical applications. Among them we can mention the study of the mechanism that generates eclipses in eclipsing binaries [9]. Concurrent observations in different frequency bands can also be exploited to compensate for the ionosphere dispersion in Pulsar survey [3]. In fact, when performing high precision timing it is important to account for the variable effect of the interstellar medium along the line-of-sight to the source (on time scales longer than a few days). To properly remove this contribution, it is necessary to accurately measure the delay between the times of arrival of the same pulse at two well-separated frequencies. In this context, the dual-band operation of the L-P receiver allows halving the time required to obtain a

TABLE 1. Key parameters of the some of the largest radio telescopes.

Radio Telescope	Diameter (m)	Country	Frequency Range (GHz)
Green Bank (GBT)	100	USA	0.3 - 116
Effelsberg (EFF)	100	Germany	0.3 - 96
Tianma (TMRT)	65	China	1.25 - 50
Sardinia (SRT)	64	Italy	0.3 - 116
Parkes (PARKES)	64	Australia	0.7 - 25
Nobeyama (NOB)	45	Japan	20 - 116
Yebes (YEB)	40	Spain	2 - 116
Medicina (MED)	32	Italy	1.35 - 26.5
Noto (NOTO)	32	Italy	1.4 - 86

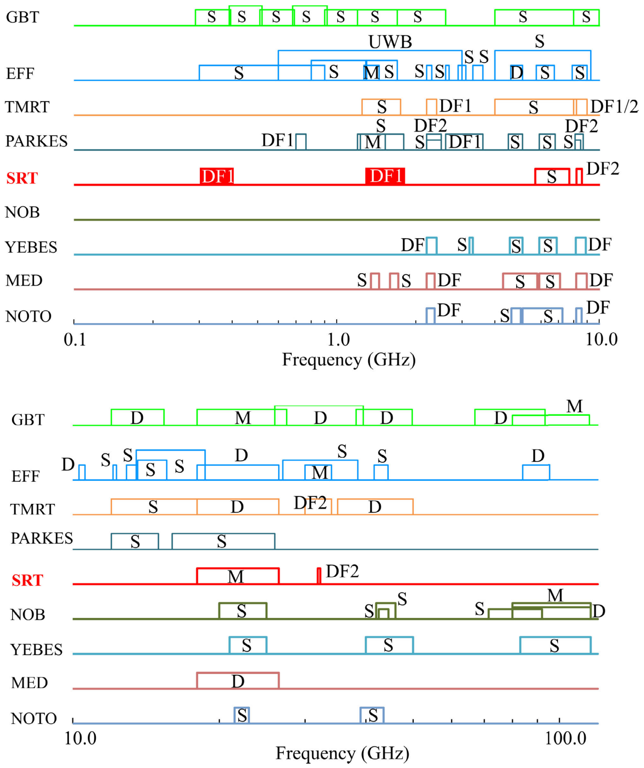

FIGURE 2. Frequency coverage and category of large radio telescope receivers. S = mono-feed; D = dual-feed; M = multi-feed; DF = dual-frequency; UWB = UWB-feed. The two bands of dual-frequency receivers are identified with the same number.

high precision timing of a target, which in turn, implies the possibility to double the number of useful observations for the given target (in an assigned telescope time).

The coaxial L-P receiver of SRT can also be used to observe a radio source with a single band. For example, the VLBI observations require L-band operation [10]. Recently, from 20 to 24 February 2020, the P-band receiver has been used to perform the lowest-frequency detection to date of three radio bursts, observed at 328 MHz from the periodic repeater FRB 180916.J0158 + 65 [11]. Simultaneous observations with the L-band receiver at 1548 MHz were also performed but did not detect any bursts. A further application of the SRT in the P band channel (and linear polarization) is space debris detection, as the receiving part of the BIRALET bistatic radar [6]–[8].

The bandwidth of the L-P receiver has been chosen after astronomical considerations but also primarily after Radio Frequencies Interference (RFI) measurement around the SRT site. Indeed, at the start of the project the P-band was supposed to cover the frequency range 305-425 MHz, but after several RFI campaigns, it was decided to narrow down the band to the present frequency range, i.e. 305-410 MHz. Based on the same considerations, the operating frequency range of the L-Band has been selected between 1.3 GHz - 1.8 GHz to achieve the widest radio astronomical performance, while avoiding adjacent-channel interference. The RFI monitoring is performed periodically to identify any possible new source of interference [12].

II. ARCHITECTURE OF THE L-P RECEIVER

The L-P receiver is installed on the primary focal position F1. For this reason, it must meet strong weight and dimension constraints: it has a volume of about 1.5 m × 1.5 m × 1.5 m and a weight of 700 Kg.

Because of its relatively low operating frequency range, this receiver is characterized by the absence of the mixer section. Indeed, the two RF bands (P-band and L-band) are inside the intermediate frequency (IF) of the SRT, which covers the frequency range 0.1 - 2.1 GHz [13]. As a consequence, the down-conversion of the RF bands is not required.

The main features of the receiver are listed in the following:

- Frequency range: 305-410 MHz (P-band) and 1.3-1.8 GHz (L- band) simultaneously.
- Linear and circular polarization for each frequency band.
- System Temperature (T_{REC}) $\sim$ 20 K in the P-band and $\sim$10 K in the L-band.
- Selectable linear or circular polarization for specific observations.
- Selectable narrow band for VLBI observations.

The basic architecture of the receiver is shown in Fig. 3(a), wherein we report the main blocks and components that form the front-end path. Starting from the left side of the figure we can find:

a) The coaxial feed converting the received (P-band or L-band) free-space electromagnetic wave into a guided wave, operating at environmental temperature (300 K).
b) The coaxial orthomode junction (OMJ) of the P-band receiver, which is integrated in the coaxial feed and works at room temperature (300 K).
c) The cryostat (or Dewar), wherein some of the components of the P-band and L-band receiver paths are housed, operating at the temperature of 20 K.
d) The noise calibration unit, which provides the receiver calibration for both L and P frequency bands by injecting a noise source in the RF paths. The block diagram is described in Fig. 3(a).
e) The P-band linear to circular polarizer (Fig. 3(b)).
f) The L-band linear to circular polarizer (Fig. 3(b)).
g) The P-band filter selector, which allows selecting narrow-bands within the P-band for specific radio astronomy observations. The block diagram is shown in Fig. 3(c).
h) The L-band filter selector, which allows selecting narrow-bands within the L-band for specific radio astronomical observations (Fig. 3(d)).

In the following subsections we will describe in detail the design and the architecture of the blocks a), b), and c) listed above.

A. ARCHITECTURE OF THE COAXIAL FEED

The feed of the dual-band L-P receiver is realized using a coaxial configuration, which includes also the coaxial orthomode junction (OMJ) of the P-band. The latter operate at room temperature (300 K), whereas the OMJ of the L-band works at cryogenic temperature (20 K) (see Fig. 3(a)). The design of the P- and L-band feeds and of the P-band OMJ have been made using the commercial software CST Studio Suite. The section view and 3D view of these components are shown in Fig. 4.

The P-band OMJ and the P-band feed consist of a coaxial waveguide with an outer diameter equal to $D_P = 650$ mm (which is the P-band feed aperture, as well), and a variable inner diameter, which corresponds to the L-Band waveguide and is composed of three sections: a first section, starting from the back-short, of length $L_1 = 575$ mm and diameter $D_{L1} = 196$ mm; a matching conical section of length $L_2 = 120$ mm; a third section, terminating at the feed aperture, with length $L_3 = 220$ mm and diameter $D_{L2} = 171$ mm (see Fig. 4).

Four matching cylindrical metallic irises are arranged along the optical axis of the P-band feed. Two of them, I1 and I2, are attached to the inner L-band waveguide near to the planar back-short (see Fig. 4). The other two metallic irises, I3 and I4, are located near the aperture of the feed: one is attached to the external P-band waveguide, the other is attached to the internal L-band waveguide (Fig. 4). The dimensions of these irises are reported in Table 2, wherein L_{Ii} is the distance of the iris Ii from the backshort, and T_{Ii} is the thickness of the iris Ii (Fig. 4).

The sketch of the P-band orthomode transducer (OMT), which includes the coaxial OMJ and two 180° Hybrid power dividers, is shown in Fig. 5 (only one polarization).

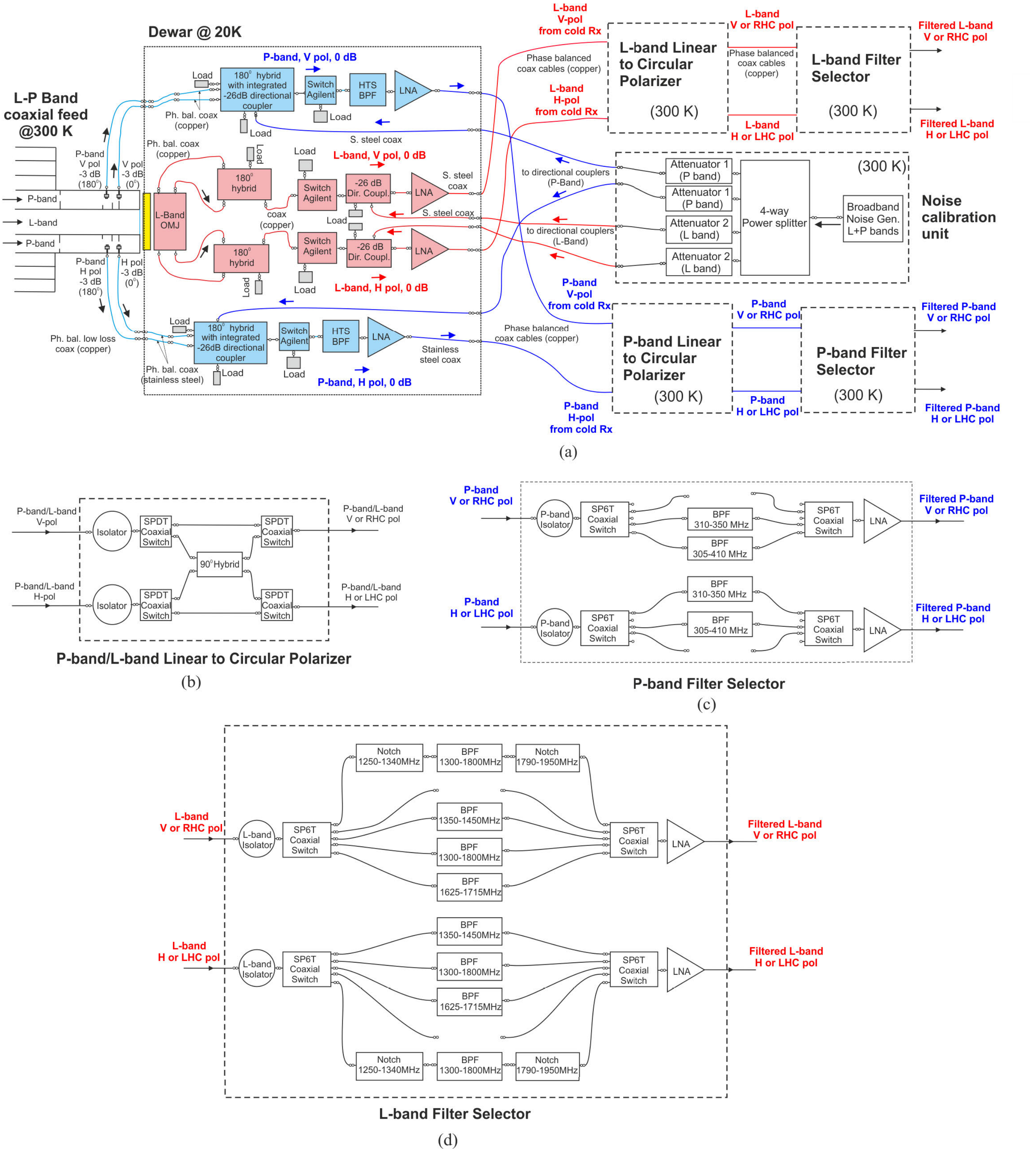

(a)

(b)

(c)

(d)

FIGURE 3. Front-end architecture of the coaxial dual-band L-P receiver.

Two linear polarized signals (Pol. 1 and Pol. 2) are extracted through four identical metallic coaxial probes connected to the central pin of commercial 50 Ω 7/16-type coaxial connectors (Fig. 6(b)). The probes are located at $L_{I1} = 177.5$ mm from the back-short of the coaxial waveguide and each one consists of four cylinders of different diameters with the same axis of the coaxial connectors. The geometry, the position and the dimensions of the probes have been optimized for a better matching and are reported in Fig. 6(c). To avoid mechanical microphonics problems due both to the radio telescope movement and to the vibration of the cryogenic pump, the inner part of the probes has been

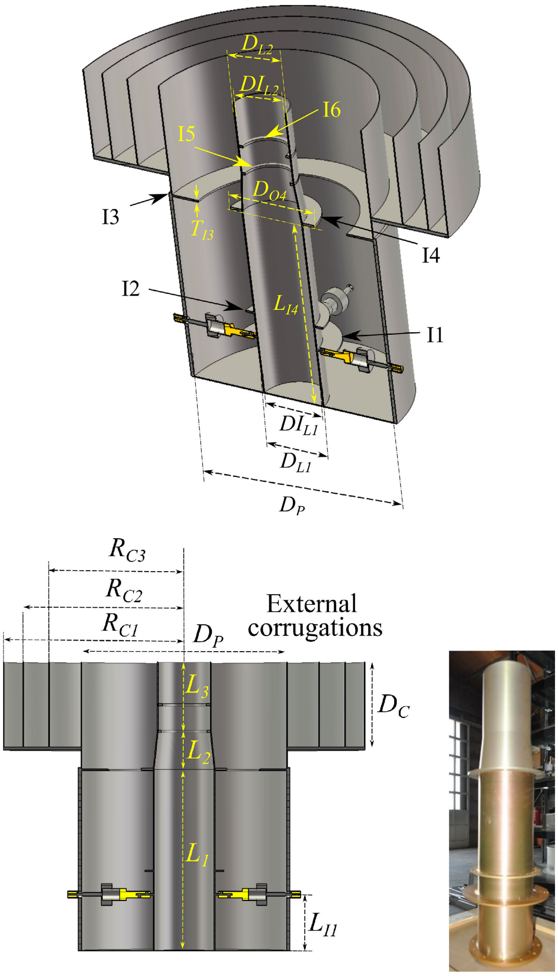

FIGURE 4. Section view and 3D view (CST Studio Suite Model) of the coaxial L-P feed and OMJ.

TABLE 2. Geometry of the matching irises in the L-P feed.

Band	Iris	D_{OUTER} [mm]	D_{INNER} [mm]	Thickness [mm]	Distance [mm]
P	I1	$D_{O1} = 305$	$D_{I1} = D_{L1}$	$T_{I1} = 5$	$L_{I1} = 177.5$
	I2	$D_{O2} = 250$	$D_{I2} = D_{L1}$	$T_{I2} = 5$	$L_{I2} = 252.5$
	I3	$D_{O3} = D_P$	$D_{I3} = 480$	$T_{I3} = 5$	$L_{I3} = 572.5$
	I4	$D_{O4} = 272$	$D_{I4} = D_{L1}$	$T_{I4} = 7$	$L_{I4} = 574.5$
L	I5	$D_{O5} = DI_{L2}$	$D_{I5} = 145$	$T_{I5} = 7$	$L_{I5} = 694.5$
	I6	$D_{O6} = DI_{L2}$	$D_{I6} = 139$	$T_{I6} = 7$	$L_{I6} = 779.5$

hollowed and fixed to one of the irises (I1) through robust Teflon ($\varepsilon_r = 2.01$) supports. This solution allows reducing the weight of the probes as well.

The fundamental mode of the coaxial waveguide described so far is the TEM mode and the cut-off frequency of the first higher order mode, the TE_{11}, is 232 MHz. However, using the four-probes OMJ feeding configuration, the fundamental TEM mode does not propagate. Under these conditions, in the operating P-band of the receiver (305 MHz – 410 MHz), only the TE_{11} mode propagates and its wavelength at the center frequency (357.5 MHz) is about $\lambda_g = 1100$ mm.

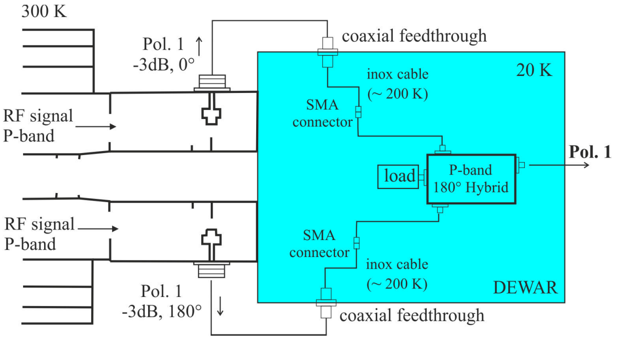

FIGURE 5. Sketch of the P-band feed and OMT. An identical configuration not shown here is present for the orthogonal polarization.

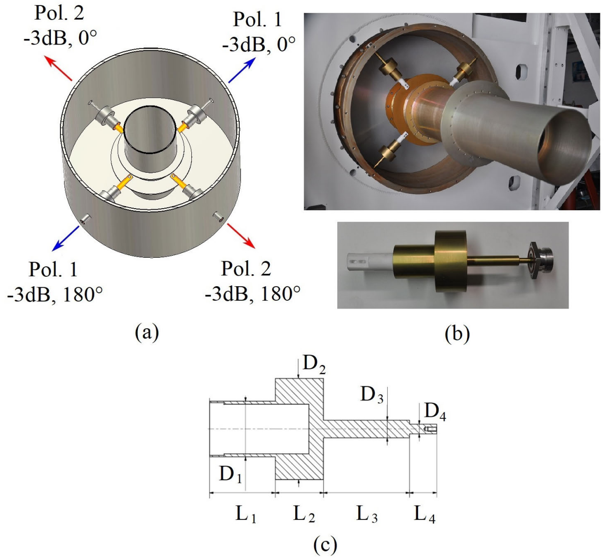

FIGURE 6. P-band OMJ: (a) CST model; (b) photo of the coaxial waveguide with detail of the probes; (c) geometry of the probe: $L_1 = 45$ mm, $L_2 = 33$ mm, $L_3 = 59$ mm, $L_4 = 18$ mm, $D_1 = 38$ mm, $D_2 = 59$ mm, $D_3 = 12$ mm, $D_4 = 6.5$ mm.

Finally, to improve the radiation pattern of the P-band feed external corrugations have been placed on the aperture flange. They are composed of three rings with a maximum diameter of 1148 mm and a thickness of 2 mm each. The distances of the throats from the optical axis are: $R_{C1} = 574$ mm, $R_{C2} = 510$ mm, and $R_{C3} = 428$ mm, with a depth of $D_C = 320$ mm (see Fig. 4).

The L-band feed is a simple truncated circular waveguide, which is inside the circular waveguide of the P-band feed (see Fig. 4). As pointed out before, this waveguide is made of three sections (Fig. 4): a section "A" of length L_1 and constant diameter, a matching conical section "B" of length L_2, and section "C" of length L_3 and constant diameter. The waveguide wall thickness is 3 mm. Therefore, the inner diameter of sections "A" and "C" is $DI_{L1} = 190$ mm and $DI_{L2} = 165$ mm, respectively. The structure has one physical port but two electrical ports because two degenerate TE_{11} modes are excited inside the circular waveguide [14].

Two irises, I5 and I6, located near the aperture of the feed (Fig. 4), have been used to match the free space impedance

FIGURE 7. **Photo of the coaxial feed.**

to the impedance of the circular waveguide. The dimensions and position of the irises are listed in Table 1, whereas the diameter reduction (from DI_{L1} to DI_{L2}) is aimed to improve the return loss of the OMJ [14].

The photo of the L-P feed installed on the primary focus of SRT is shown in Fig. 7.

B. P-BAND RECEIVER CRYOGENIC RF PATH

As discussed in Section II.A, the coaxial orthomode junction of the P-band receiver is integrated into the coaxial feed and operates at room temperature (300 K). On the other hand, the components of the P-band receiver, cascaded as shown in Fig. 3(a) and operating at a cryogenic temperature of 20 K, are:

- A cryogenic 180° hybrid with integrated directional coupler [15]. A planar fractal 180° hybrid configuration has been used to cover the operating bandwidth of the receiver with a significant size reduction, which is mandatory to save space (and refrigerating power) inside the cryostat. The return loss is larger than 20 dB over the operating bandwidth, whereas amplitude and phase imbalance are 0.5 dB and ±10°, respectively. A coupled lines directional coupler with weak coupling (−26 dB) and high isolation (below −45 dB), used to calibrate the receiver chain, is cascaded to the 180° hybrid and realized in the same layout. The planar size of the resulting six-port component is only 108 mm × 160 mm. This component has been successfully tested at the cryogenic operating temperature (20 K), with a percentage power loss of less than 1.5% over the operating frequency band.
- A commercial cryogenic coaxial mechanical switch (model Agilent 8761B). It is used to isolate the P-band low noise amplifier (LNA) should the SRT be equipped in the future with a transmitter for deep space and near-earth applications. The insertion loss of this component is estimated at 0.01 dB at 20 K and the equivalent noise temperature is negligible.
- A cryogenic bandpass filter, which is proposed in [16]. Typically, a filter is not used before the LNA in the RF path since its insertion loss worsens the system temperature of the whole receiver. However, in our case, the band pass filter has been used to reject a strong radio frequency interference near 420 MHz, which is slightly outside the receiver bandwidth. This filter has been designed with a high-temperature superconducting (HTS) technology to reduce the losses before the LNA. A magnesium oxide substrate with a thickness of 0.503 mm and a dielectric permittivity of 9.65 has been used. The superconducting transmission lines are made by yttrium barium copper oxide (YBCO). The metallic box has been realized in (gold-plated) titanium to match the thermal expansion of the substrate. The insertion loss of this device is about 0.09 dB (plus a ripple of 0.12 dB) at 20 K and the equivalent noise temperature is less than 1 K.
- A cryogenic LNA. The LNA designed in [17] has been used for the P-band receiver. The input and output matching are, respectively, better than 10 dB and 20 dB in the operating bandwidth. The measured gain is 27 dB at the center frequency and the noise temperature at 20 K is less than 5 K in the operating bandwidth.

C. L BAND RECEIVER CRYOGENIC RF PATH

A 125μm thick Kapton vacuum barrier (with dielectric permittivity 3.5 and tan$\delta = 0.001$) and suitable thermal gaps [14] separate the L-band feed, at environmental temperature (300 K), from the cryogenic part of the receiver. The components of the L-band receiver operating at a cryogenic temperature of 20 K, cascaded as shown in Fig. 3(a), are:

- The orthomode transducer [14], [18], which consists of a cylindrical orthomode junction (OMJ), and two identical 180° hybrid power combiners in a double ridged waveguide (DRWG). This component provides isolation of 40 dB, cross-polarization less than −35 dB, and an estimated noise temperature less than 1.3 K at the cryogenic temperature of 20 K.
- A commercial cryogenic switch (model Agilent 8761B) used to isolate the L-band LNA in case the SRT should be equipped in the future with a transmitter for deep space and near-earth applications.
- A cryogenic microstrip directional coupler with high directivity, low insertion loss (less than 0.16 dB) and weak coupling (−26 dB at the center frequency), employed to calibrate the L-band receiver chain by injecting a noise source and a weak coherent comb signal in the RF path [19].
- A cryogenic LNA. The LNA designed in [20] has been used for the L-band receiver. This LNA is composed of three cascaded high electron mobility transistors. The input and output matching are, respectively, better than 10 dB and 15 dB in the operating bandwidth. The measured gain is 38 dB at the center frequency and the noise temperature at 20 K is less than 4 K in the operating bandwidth.

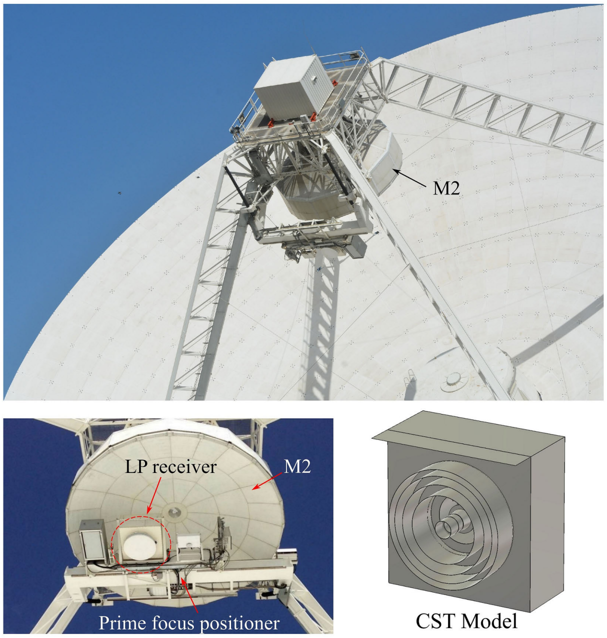

FIGURE 8. **Photos of the L-P receiver installed on the SRT and CST model including the protective metallic box containing the receiver and a frame to simulate the presence of the primary focus positioner.**

TABLE 3. **Radiation properties of the P band feed (45° cut).**

Frequency [MHz]	Gain [dBi]	X-pol [dB]	Edge Taper [dB]
305	9.4	-28	-13.0
357	9.9	-30	-15.2
410	10.4	-27	-17.2

III. RADIATION PERFORMANCE OF THE COAXIAL L-P FEED

In this section we analyze and discuss the performance of the L-P band feed. All the simulations presented here have been performed using CST studio Suite.

Photos of the receiver installed on the SRT and the CST model of the feed are reported in Fig. 8. The effect of the metallic box containing the receiver has been considered in the CST simulations, and a metallic frame has been added to the model to account for the presence of the prime focus positioner (Fig. 8).

In Fig. 9 the simulated radiation pattern in the principal planes (E-plane, 45°, and H-plane cuts) and the cross-polarization (45° cut) is reported at the center frequency (357 MHz). Table 3 summarizes the feed gain, the cross-polarization level, and the taper at the edges of the SRT aperture (which corresponds to 74°) at 357 MHz and at the ends of the operating P-band.

The optimum theoretical value of edge taper for the SRT is about −12 dB at 74 degrees. However, we have designed the feed with a value of the edge taper slightly lower with respect to the theoretical value of −12 dB to reduce the effect of the spill over. The consequence is a slight under-illumination of the primary mirror.

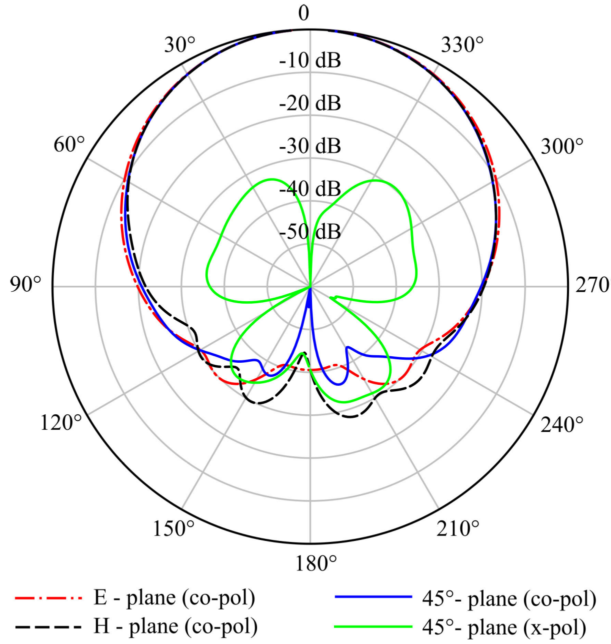

FIGURE 9. **Simulated normalized radiation pattern of the P-band feed at 357 MHz.**

Finally, the improvement of the P-band feed radiation pattern due to the external corrugations (see Fig. 4 and Section II.B) has been evaluated by CST simulations. In Fig. 10, we compare the radiation pattern of the feed at the center frequency of 357 MHz with or without these corrugations. The position of the corrugations has been optimized using the CST model reported in Fig. 4, i.e. without the metallic box containing the receiver. The simulations show that a reduction larger than 10 dB of both the back-radiation and the cross-polarization can be observed thanks to the choking effect of the corrugations.

We conclude the discussion on the P-band feed with an experimental assessment of the OMJ, which is included in the same guiding structure of the feed, as reported in Section II.A. This component has been characterized by means of the output return loss measurement, whereas the insertion loss and the cross-polarization have been estimated using CST simulations and theoretical considerations.

The experimental setup for the measurement of the output return loss is shown in Fig. 11. The reflection from the coaxial output of the OMJ has been obtained by terminating the coaxial waveguide input with an Eccosorb® load. The return loss, measured using a Vector Network Analyzer connected at the output of a commercial 180° power splitter, is reported in Fig. 12 and compared with simulated results. The agreement between simulation and measurement is excellent and the reflection is below −20 dB in the operating bandwidth.

The OMJ of the L-band receiver has been extensively tested both with simulations and measurements in [14] and

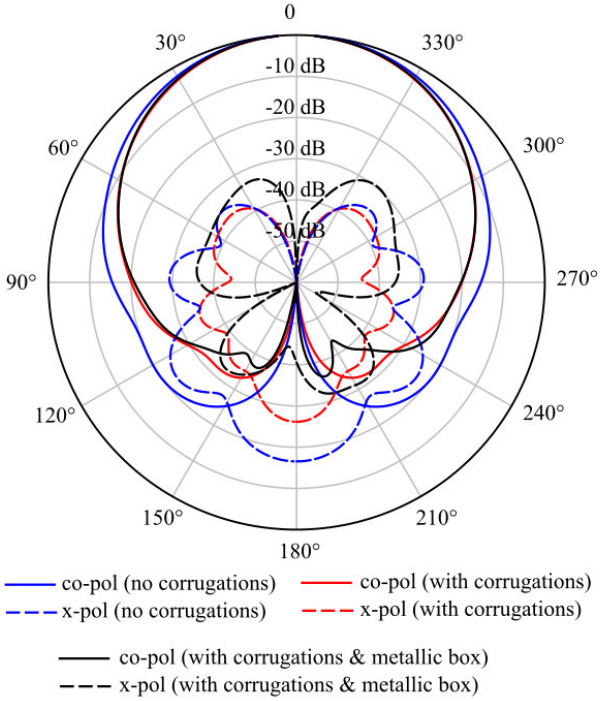

FIGURE 10. Simulated normalized pattern of the P-band feed at 357 MHz (45° plane) with and without external corrugations.

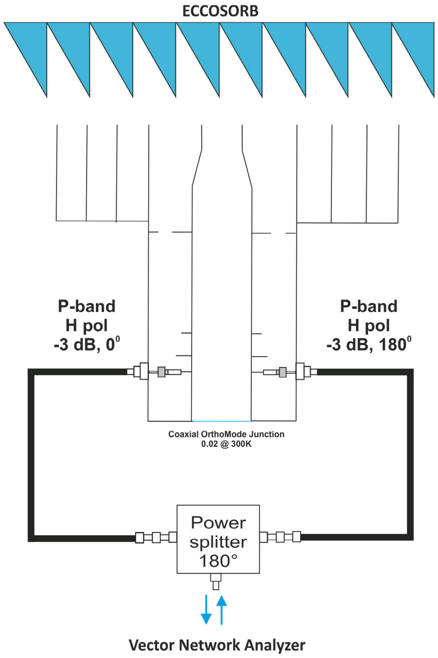

FIGURE 11. Return Loss Measurement setup of the P-band coaxial OMJ (single polarization).

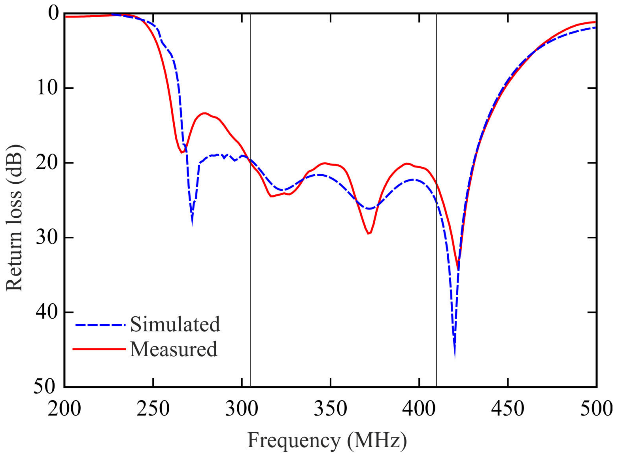

FIGURE 12. Return loss of coaxial ortho mode junction.

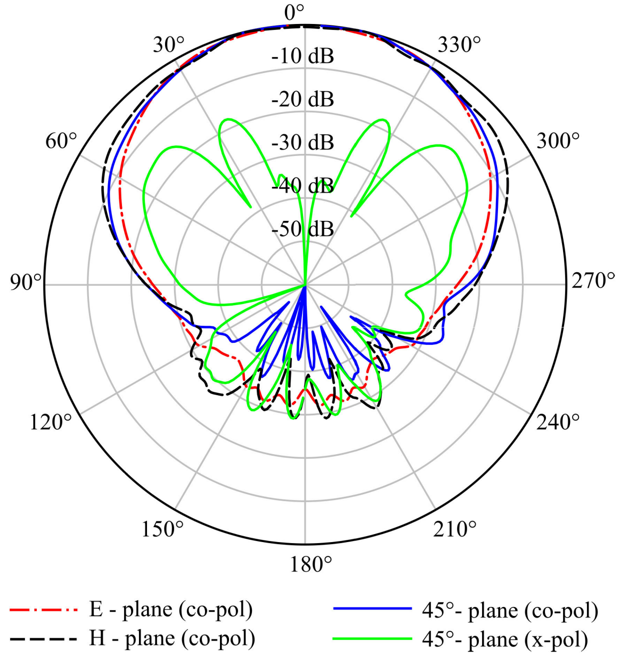

FIGURE 13. Simulated normalized radiation pattern of the L-band feed at 1.55 GHz.

TABLE 4. Radiation properties of the L band feed (45° cut).

Frequency [MHz]	Gain [dBi]	X-pol [dB]	Edge Taper [dB]
1300	10.4	-23.0	-14.9
1550	9.0	-15.0	-14.6
1800	10.0	-19.5	-18.0

its performance has been summarized in section II.C. Therefore, we focus here on the far-field pattern of the feed in the L-band. In Fig. 13 the simulated radiation pattern in the principal planes (E-plane, 45°, and H-plane cuts) and the cross-polarization (45° cut) is reported at the center frequency (1550 MHz), whereas table 4 summarizes the feed gain, the cross-polarization, and the edge taper at 74° at 1550 MHz and at the ends of the operating L-band. As made for the P-band, the L-band feed has also been designed with an average value of the edge taper slightly lower than the theoretical value of -12 dB to reduce the effect of the spill over.

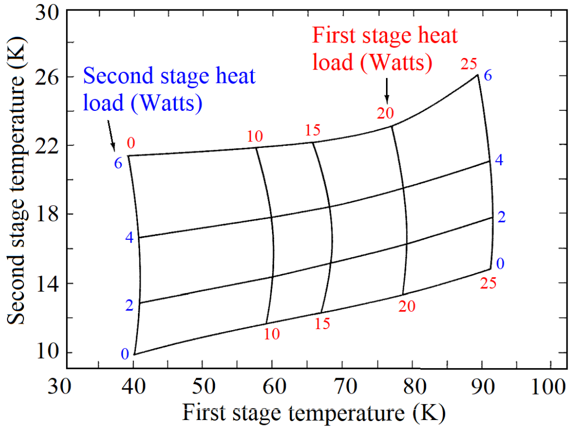

FIGURE 14. Refrigeration capacity of the model 350C Cryodyne® cryocooler (60 Hertz).

IV. THERMAL DESIGN OF THE CRYOSTAT

To reduce the system noise temperature some devices of the receiver chain have been housed inside a cryostat, a vacuum container with inner coaxial radiation shields, to operate at cryogenic temperature (see Fig. 3(a)). The cryogenic system consists of a two-stage commercial cryocooler (model 350C Cryodyne® [21]). We have set the upper nominal temperatures of the two stages at 20 K and 77 K, respectively. As shown in Fig. 14, the desired physical temperatures are obtained when the heat power dissipation is less than 20 W on the first stage and less than 4 W on the second stage.

To obtain an estimate of the cooling power required by the cylindrical Dewar fabricated for the L-P receiver, a complete cryostat was thermally modeled. We divided the thermal model of the Dewar into three stages: "stage 0" (at 300 K), "stage 1" (at 77 K), and "stage 2" (at 20 K). Basically, three physical phenomena contribute to the thermal load: convection, radiation, and conduction.

Since the typical pressure inside the Dewar is below 10^{-7} mBar, the contribution of the convection has been neglected [22].

The thermal radiation [22], [23] depends mainly on the radiating surface of the Dewar and on the emissivity of the material used to fabricate it (aluminum in our case) [22]. The thermal radiation has been reduced using additional "thermal shields" made of a cylindrical 2mm-thick structure in aluminum coated with a sheet of polyester superinsulation, composed of 10 layers (e.g. type COOLCAT 2 by RUAG). We have employed two thermal shields, the first between "stage 0" (at 300 K) and "stage 1" (at 77 K), the second between "stage 1" and "stage 2" at 20 K (see Fig. 15).

The major thermal contribution due to radiation comes from the L-band OMJ [14] (Fig. 16), which operates at 20 K. Indeed, the backshort of the OMJ "sees" the conically tapered section of Styrodur® 3035 CS at higher temperature (∼300 K) as shown in Fig. 16(c). Clearly, thermal shields cannot be used in the internal circular waveguide. Using the emission coefficients of the Styrodur® 3035 CS (estimated equal to 0.08-0.1) and of the aluminum (about 0.05), the radiation contribution has been overestimated to about 0.7 Watts [23], [24].

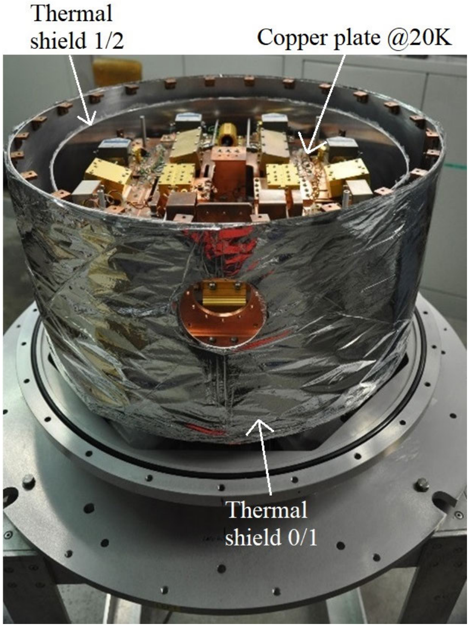

FIGURE 15. Detail of the fabricated cryostat: view of the thermal shields between "stage 0" and "stage 1"and between "stage 1" and "stage 2."

Then, we need to account for the thermal conduction [23], [24]. Four main contributions should be considered:

i) The thermal conduction across the four cylindrical columns of G10 material, used to sustain the mechanical parts of "stage 0" and "stage 1," which are separated by a small air-gap (Fig. 16(a)) [14].
ii) The thermal conduction across the four (flat and holed) supports of G10 employed as a support for the air-gap between "stage 1" and "stage 2" (Fig. 16(a)) [14].
iii) The thermal conduction across the four cylindrical columns of G10 material used to sustain the copper plates at 20 K (Fig. 16(b)) wherein the cryogenically cooled devices are housed (Fig. 15) [14].
iv) The thermal conduction due to the coaxial cables employed in the P-band and L-band RF paths.
v) The thermal conduction due to the electrical connections.

The contribution of the G10 supports has been estimated by thermal simulations of the OMJ performed with the commercial software Solidworks, whereas the contribution of the coaxial cables and electrical connections has been computed through analytical expressions derived by [22]–[25].

Finally, the thermal load due to the power dissipation of the cryogenic LNAs should be considered.

The results of the thermal analysis are summarized in table 5, showing a total thermal load of 3.8 W and 2.5 W, respectively for stage 1 and stage 2, well below the heat power dissipation limits of the cryocooler (Fig. 14).

TABLE 5. Thermal budget of the cryostat.

		Stage 1 (77 K)	Stage 2 (20 K)
Thermal radiation	1st Thermal Shield	< 1 W	-
	2nd Thermal Shield	-	< 10 mW
	OMJ	-	< 0.7 W
Thermal conduction	G10 columns & supports	0.4 W	0.16 W
	Coaxial cables (P-band)	1.52 W	0.82 W
	Coaxial cables (L-band)	-	0.225 W
	Electrical wires	0.76 W	0.46 W
Active devices	LNAs	0.13 W	0.18 W
TOTAL		~ 3.8 W	~2.5 W

We have placed three thermal sensors into the cryostat to monitor the temperatures of the inner stages. A sensor monitors the temperature of the first stage (nominal at 77 K) and it is placed on the aluminum plate at 77 K (see Figure 16(a)), two other sensors monitor the temperature of the second stage (nominal at 20 K) and are installed on the P-band LNA and on the L-band LNA. In Fig. 17 the cooldown curve is reported. It shows that the two sensors near the LNAs measure a temperature below 20 K, and the sensor on the aluminum plate measures a temperature around 70 K, as required by the thermal design and predicted by our thermal analysis.

V. EVALUATION OF THE RECEIVER SYSTEM TEMPERATURE

The overall noise temperature of the receiver (T_{REC}) is one of the key parameters of the front-end. Its value impacts the system noise temperature, which includes the atmospheric contribution and the spillover, and consequently the sensitivity achieved during radio astronomy observations [26]. Each component of the P-band and L-band RF paths described in section II has been characterized with measurement, simulations, and/or theoretical considerations to estimate the final noise temperature of the P-band and L-band receivers. For each passive component of the receiver chain, the equivalent noise temperature has been computed by

$$T_{ei} = T_{REFi}\left(10^{\frac{NFi(dB)}{10}} - 1\right) \tag{1}$$

wherein T_{REFi} is the physical temperature of the component and NF_i its noise figure. Then, the final noise temperature of the receiver T_{REC} has been computed using the well-known Friis formula for n cascaded blocks [26], [27]:

$$T_{REC} = T_{e1} + \frac{T_{e2}}{G_1} + \frac{T_{e3}}{G_1 \cdot G_2} + \cdots + \frac{T_{en}}{G_1 \cdot G_2 \cdot \cdots \cdot G_n} \tag{2}$$

where T_{ei} and G_i are the noise and the available power gain of the i^{th} stage. The predicted values of the T_{REC} are reported in Table 6 for the P-band receiver and in Table 7 for the L-band receiver.

The estimated values of the system noise temperature of the receiver reported in Table 6 and 7 have been assessed by measurements, for both receivers (P-band and L-band) and both polarization channels (Horizontal and Vertical).

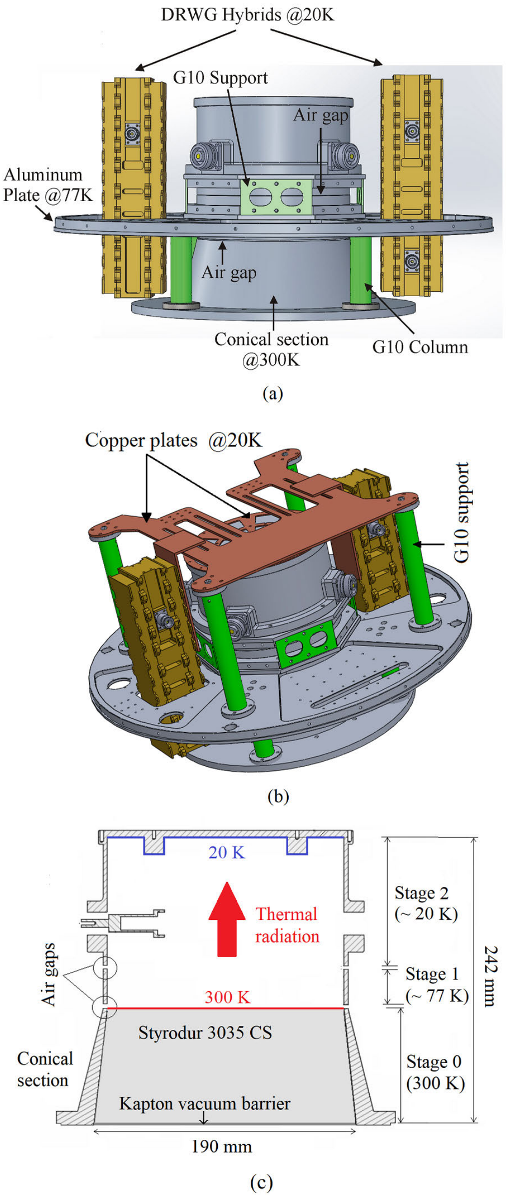

FIGURE 16. 3D view of the L-band OMJ and DRWG 180° hybrids (a and b): the DRWG Hybrids and the backshort of the OMJ are connected to copper plates @ 20K (not shown in (a)), the DRWG hybrids pass through holes in the aluminium plate at 77 K (b), without any contact with this plate; (c) cross-section of the OMJ; for more details and geometrical dimensions of the L-band OMJ see [14].

The Y-factor method [28] has been used to perform these measurements. The Y-factor is the ratio of two noise power levels, measured by switching on/off a suitable noise source. These two measurement points are employed to draw a line representing the linear noise power as a function of the noise temperature. Finally, the Y-intercept at the temperature of the device under test (DUT) indicates the noise added by the DUT.

In our case, the required power levels are generated by switching between a load at room temperature (300 K) and the Maury Microwave MT7118A Cryogenic Termination

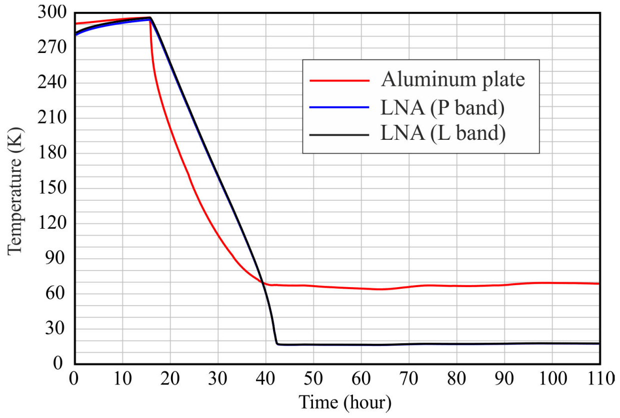

FIGURE 17. Cooldown curve of the coaxial receiver.

TABLE 6. Estimated T_{REC} of the P-band receiver. The components are divided by blocks (see Fig. 3). F = free-space; DW = Dewar; POL = Polarizer; FS = Filter selector.

Component	Block (Fig. 3)	T_{REF} (K)	Gain /Loss (dB)	NF (dB)	T_e (K)
Coax-Feed & OMJ	F	300	-0.01	0.01	0.7
Cable FSJ-50	F	300	-0.09	0.09	6.3
Cable Stainless Steel	DW	160	-0.1	0.1	3.7
Cable Cu	DW	20	-0.18	0.18	0.8
180°Hybrid & Dir. C.	DW	20	-0.27	0.27	1.3
BP filter & Switch	DW	20	-0.21	0.21	1.0
LNA	DW	20	27		5
Cable Stainless Steel	DW	160	-0.2	0.2	7.5
Cable Cu	F	300	-0.4	0.4	28.9
Isolator	POL	300	-0.4	0.4	28.9
Switch	POL	300	-0.31	0.31	22.2
90° Hybrid	POL	300	-0.2	0.2	14.1
Switch	POL	300	-0.31	0.31	22.2
Isolator	FS	300	-0.4	0.4	28.9
Switch	FS	300	-0.2	0.2	14.1
Band-pass filter	FS	300	-0.6	0.6	44.4
Switch	FS	300	-0.2	0.2	14.1
LNA	FS	300	28	2.05	181
T_{REC} (K)					**22.1**

Chamber, which provides a load at 77 K. Then, the system noise temperature of the receiver at 20 K has been extrapolated, and the results are reported in Table 8 and 9. An excellent agreement with the T_{REC} estimated in Table 6 and 7 can be observed for both polarizations and at different frequencies.

The noise temperature of the L-P receiver of the SRT has been assessed against the noise performance of the receivers of other large radio telescopes for radio astronomy (Table 1) in the frequency range of interest. The results reported in Fig. 18 show the good performance of the proposed coaxial dual-frequency receiver in comparison with the receivers available in the main radio astronomical facilities.

VI. COUPLING BETWEEN THE COAXIAL FEED AND THE SARDINIA RADIO TELESCOPE

To compute the reflector antenna gain, efficiency, and cross-polarization, the coupling between the coaxial L-P feed and the SRT has been evaluated using the commercial software GRASP by Ticra. GRASP is a reliable tool for the analysis and design of reflector antenna systems, which employs an advanced Physical optics (PO) algorithm as the baseline analysis method, supplemented by Geometrical Theory of Diffraction (GTD) and Moment Method (MoM) solvers for advanced applications. In the GRASP model of the SRT we

TABLE 7. Estimated T_{REC} of the L-band receiver. The components are divided by blocks (see Fig. 3). F = free-space; DW = Dewar; POL = Polarizer; FS = Filter selector.

Component	Block (Fig. 3)	T_{REF} (K)	Gain /Loss (dB)	NF (dB)	T_e (K)
Circular Feed	F	300	-0.02	0.02	1.4
Vacuum Window	F	300	-0.01	0.01	0.7
OMJ	DW	20	-0.20	0.20	0.9
Cable Cu	DW	20	-0.04	0.04	0.2
DRWG 180° Hybrid	DW	20	-0.04	0.04	0.2
Cable Cu	DW	20	-0.04	0.04	0.2
Switch & Dir. C.	DW	20	-0.18	0.18	0.8
LNA	DW	20	38		4
Cable Stainless Steel	DW	160	-0.5	0.5	19.5
Cable Cu	F	300	-1.1	1.1	86.5
Isolator	POL	300	-0.4	0.4	28.9
Switch	POL	300	-0.32	0.32	22.9
90° Hybrid	POL	300	-0.2	0.2	14.1
Switch	POL	300	-0.32	0.32	22.9
Isolator	FS	300	-0.4	0.4	28.9
Switch	FS	300	-0.2	0.2	14.1
Band-pass Filter	FS	300	-1.3	1.3	105
Switch	FS	300	-0.2	0.2	14.1
LNA	FS	300	25	1.4	114
T_{REC} (K)					**9.2**

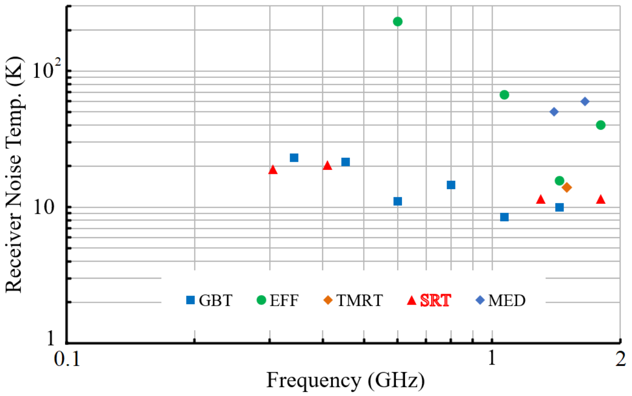

FIGURE 18. Receiver noise temperature of large radio telescope receivers up to 2 GHz.

TABLE 8. Measured T_{REC} of the P-band receiver (Y-factor method).

Frequency [MHz]	H-Polarization [K]	V-Polarization [K]
310	20	18
330	21	19
350	19	19
380	17	18
410	22	19

TABLE 9. Measured T_{REC} of the L-band receiver (Y-factor method).

Frequency [MHz]	H-Polarization [K]	V-Polarization [K]
1300	12	11
1400	10	10
1500	12	11
1600	13	11
1700	13	11
1800	12	11

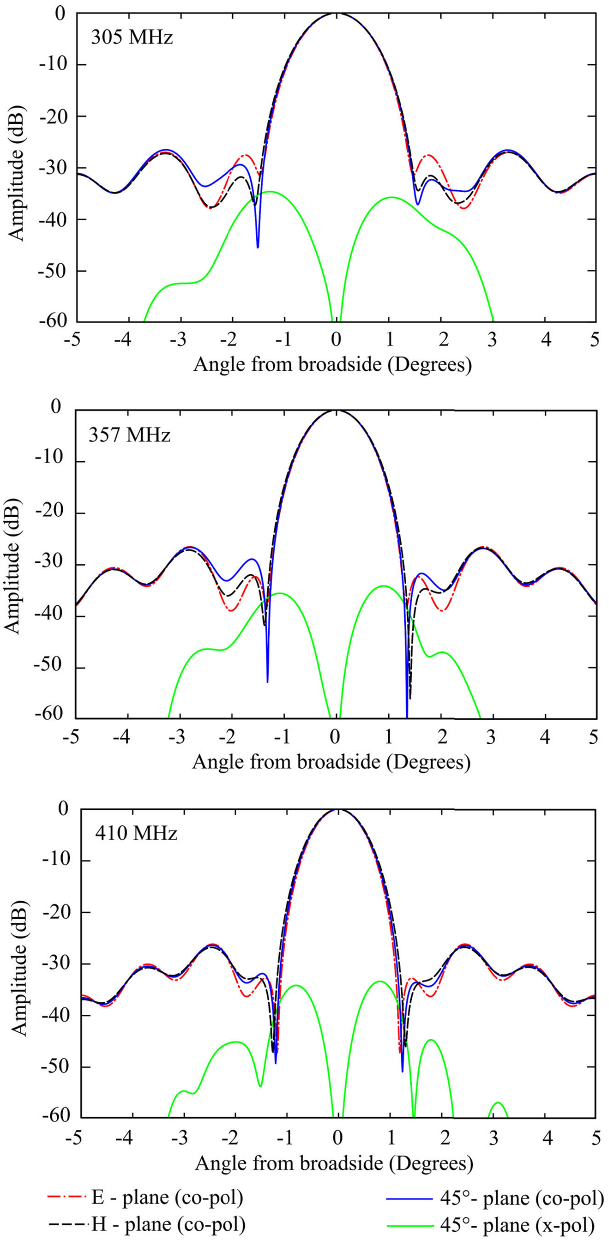

FIGURE 19. Normalized radiation pattern of the SRT illuminated with the P-band feed at 305 MHz, 357 MHz, and 410 MHz, simulated with GRASP.

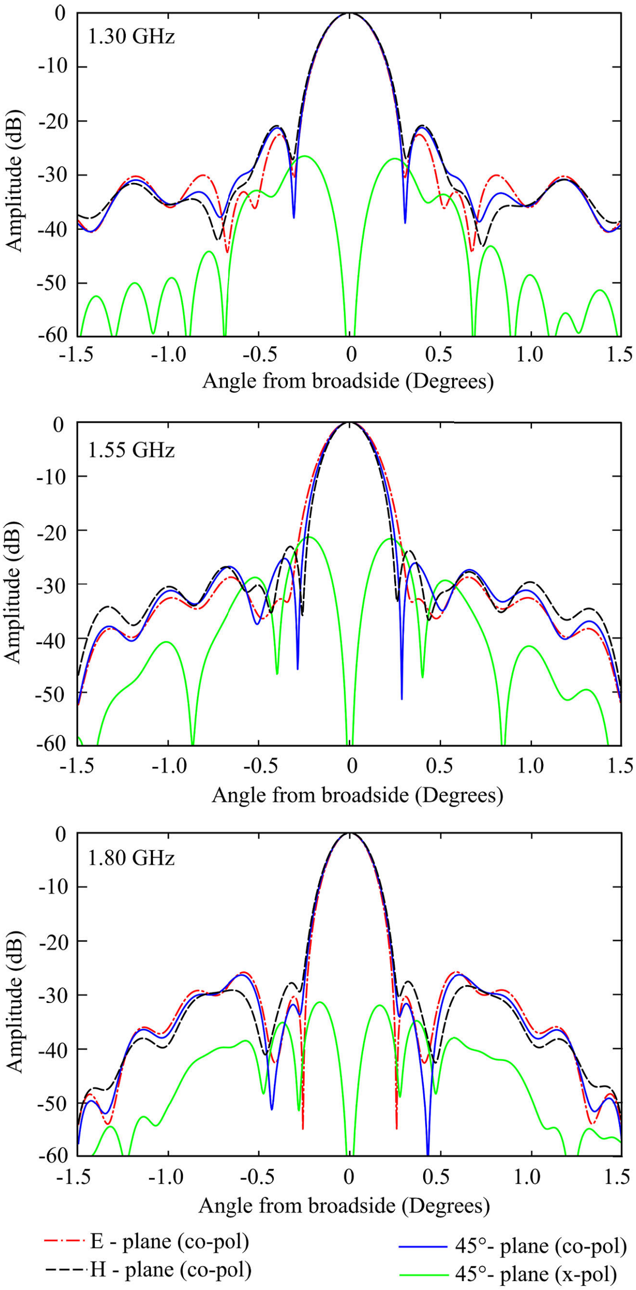

FIGURE 20. Normalized radiation pattern of the SRT illuminated with the L-band feed at 1.3 GHz, 1.55 GHz, and 1.8 GHz, simulated with GRASP.

have considered the blocking effect of both the sub-reflector (M2) and the quadrupods (see Fig. 1). At present, in the absence of measurements from a calibrated celestial radio source, the software GRASP, whose results can be considered equivalent to experiment [29], has been also used to compute the SRT beam pattern. In Figs. 19 and 20 we show the simulated radiation pattern of the SRT coupled with the P-band and L-band feeds, respectively.

The radiation features are summarized in table 10 for the P-band and in table 11 for the L-band. The cross-polarization is lower than −30 dB in the P-band and has an average value of about −25 dB across the L-band, with a worst value of −21.5 dB at 1.55 GHz. The antenna Gain reported in tables 10 and 11 is:

$$G = \eta_A \eta_S \eta_B \eta_{RL} D_M = \eta D_M \tag{3}$$

TABLE 10. Radiating features of the SRT coupled with the P-band receiver (45° cut).

Freq. [MHz]	Gain [dBi]	X-pol. [dB]	HPBW [deg.]	η_A [%]	η_S [%]	η_B [%]	η [%]
305	43.8	-34.6	1.10	68.1	95.1	90.7	56.9
357	45.0	-34.1	0.96	65.9	96.6	90.1	55.5
410	46.0	-33.4	0.86	62.7	97.7	89.5	53.0

TABLE 11. Radiating features of the SRT coupled with the L-and receiver (45° cut).

Freq. [MHz]	Gain [dBi]	X-pol [dB]	HPBW [degrees]	η_A [%]	η_S [%]	η_B [%]	η [%]
1300	56.9	-26.5	0.240	75.8	97.2	90.9	64.7
1550	58.0	-21.25	0.216	68.3	97.8	91.1	58.5
1800	59.1	-31.3	0.192	64.8	98.8	89.8	55.7

Let D the actual antenna directivity and D_M the maximum directivity of the aperture, defined as:

$$D_M = \left(\frac{2\pi R}{\lambda}\right)^2 \tag{4}$$

wherein R is the radius of the reflector aperture and λ is the free space wavelength. Then, η_A is the aperture efficiency, defined as $D = \eta_A D_M$; η_S is the spillover efficiency; η_B is the blockage efficiency; η is the overall efficiency. The values of η_A, η_S, and η_B are reported in tables 10 and 11, whereas the return loss efficiency η_{RL} has been estimated as 97% in both L-band and P-band. The Ruze RMS efficiency, the ohmic efficiency, and the cross-polarization efficiency have been neglected since they are larger than 99%. Finally, the Half Power Beamwidth (HPBW) is 0.96 deg and 0.216 deg at 357 MHz and 1.55 GHz, respectively.

VII. CONCLUSION

We have described the design of the cryogenic dual-band L-P receiver of the Sardinia Radio Telescope. This receiver is a unique instrument in the panorama of the radio receivers installed on the radio telescopes available in the world. Thanks to this equipment, the SRT is the only large radio telescope able to observe the sky concurrently in the P-band and in the L-band, but also, separately, in each of these single bands both in linear and circular polarization.

The coaxial L-P feed of the receiver has been designed using the commercial software CST Studio Suite. The measurement of the feed radiation pattern was not possible due to the difficulty of finding an appropriate anechoic environment fitting the large dimension of the antenna. However, simulations of the far-field have been performed using CST, which can be considered equivalent to experiment for a wide range of applications [30], [31]. The coupling of the coaxial feed with the SRT has been evaluated using GRASP by Ticra, a highly reliable software for the analysis and design of reflector antenna systems.

Both home-made components and commercial devices have been employed for the realization of the receiver chain. All of them have been accurately characterized by simulations and measurements. Hybrid couplers, coaxial switches, noise injection directional couplers, and low-noise amplification stages are placed inside a compact vacuum vessel and cryogenically cooled at a physical temperature of 20 K by a commercial cryocooler. Two HTS Band Pass Filters in the P-band and an OrthoMode Junction in the L-band are also cryogenically cooled inside the cryostat, allowing to achieve low noise performance. The receiver noise temperature, measured in the laboratory prior to installation of the instrument on the SRT, was in the range 17-21 K in P-band and 10-13 K in L-band. These values match closely the predicted performance.

The successful deployment of the L-P band coaxial receiver has enabled the telescope to operate in the framework of the Very Large Baseline Interferometry and Pulsar Timing networks. Furthermore, L-P band radio astronomical observations are regularly performed in single-dish mode (continuum, spectral lines, spectro-polarimetry and Pulsars), driving numerous important scientific discoveries.

This receiver, in the P-band operation has also been employed for space applications, as space debris detection and tracking, and in the near future will operate within the program *Sardinia Deep Space Antenna* by the Italian Space Agency.

REFERENCES

[1] G. Grueff, G. Alvito, R. Ambrosini, P. Bolli, A. Maccaferri, G. Maccaferri, M. Morsiani, L. Mureddu, V. Natale, L. Olmi, A. Orfei, C. Pernechele, A. Poma, I. Porceddu, L. Rossi, and G. Zacchiroli, "Sardinia radio telescope: The new Italian project," *Proc. SPIE*, vol. 5489, 2004, Art. no. 550332, doi: 10.1117/12.550332.

[2] G. Tofani *et al.*, "Status of the Sardinia radio telescope project," *Proc. SPIE*, vol. 7012, Jul. 2008, Art. no. 70120F.

[3] I. Prandoni *et al.*, "The Sardinia radio telescope-from a technological project to a radio observatory," *Astron. Astrophys.*, vol. 608, no. A40, p. 26, 2017.

[4] P. Bolli *et al.*, "Sardinia radio telescope: General description, technical commissioning and first light," *J. Astronomical Instrum.*, vol. 4, nos. 3–4, Dec. 2015, Art. no. 1550008.

[5] G. Valente *et al.*, "Sardinia deep space antenna: Current program status and results," in *Proc. 70th Int. Astron. Congr. (IAC)*, Washington, DC, USA, Oct. 2019, pp. 21–25.

[6] G. Muntoni, L. Schirru, T. Pisanu, G. Montisci, G. Valente, F. Gaudiomonte, G. Serra, E. Urru, P. Ortu, and A. Fanti, "Space debris detection in low Earth orbit with the Sardinia radio telescope," *Electronics*, vol. 6, no. 3, p. 59, Aug. 2017.

[7] G. Muntoni, L. Schirru, G. Montisci, T. Pisanu, G. Valente, P. Ortu, R. Concu, A. Melis E. Urru, A. Saba, F. Gaudiomonte, and G. Bianchi, "A space debris-dedicated channel for the P-band receiver of the Sardinia radio telescope: A detailed description and characterization," *IEEE Antennas Propag. Mag.*, vol. 62, no. 3, pp. 45–57, Jun. 2020.

[8] T. Pisanu, G. Muntoni, L. Schirru, P. Ortu, E. Urru, and G. Montisci, "Recent advances of the BIRALET system about space debris detection," *Aerospace*, vol. 8, no. 3, p. 86, Mar. 2021.

[9] D. Perrodin, M. Burgay, A. Corongiu, M. Pilia, A. Possenti, M. N. Iacolina, E. Egron, A. Ridolfi, C. Tiburzi, S. Casu, R. Concu, A. Melis, A. Pellizzoni, and A. Trois, "Pulsar science at the Sardinia radio telescope," *Proc. Int. Astronomical Union*, vol. 13, no. S337, pp. 392–393, Sep. 2017.

[10] E. Egron, A. Pellizzoni, M. Giroletti, S. Righini, M. Stagni, A. Orlati, and C. Migoni, "Single-dish and VLBI observations of Cygnus X-3 during the 2016 giant flare episode," *Monthly Notices Roy. Astronomical Soc.*, vol. 471, no. 3, pp. 2703–2714, Nov. 2017.

[11] M. Pilia *et al.*, "The lowest-frequency fast radio bursts: Sardinia radio telescope detection of the periodic FRB 180916 at 328 MHz," *Astrophys. J.*, vol. 896, no. 2, p. L40, Jun. 2020.

[12] P. Bolli, F. Gaudiomonte, R. Ambrosini, C. Bortolotti M. Roma, C. Barberi, and F. Piccoli, "The mobile laboratory for radio-frequency interference monitoring at the Sardinia radio telescope," *IEEE Antennas Propag. Mag.*, vol. 55, no. 5, pp. 19–24, Oct. 2013.

[13] A. Melis *et al.*, "Sardinia roach2-based digital architecture for radio astronomy (SARDARA)," *J. Astronomical Instrum.*, vol. 7, no. 1, Mar. 2018, Art. no. 1850004.
[14] G. Valente, G. Montisci, T. Pisanu, A. Navarrini, P. Marongiu, and G. A. Casula, "A compact L-band orthomode transducer for radio astronomical receivers at cryogenic temperature," *IEEE Trans. Microw. Theory Techn.*, vol. 63, no. 10, pp. 3218–3227, Oct. 2015.
[15] A. Ladu, G. Montisci, G. Valente, A. Navarrini, P. Marongiu, T. Pisanu, and G. Mazzarella, "High-performance cryogenic fractal 180° hybrid power divider with integrated directional coupler," *Radio Sci.*, vol. 52, no. 6, pp. 757–766, Jun. 2017.
[16] P. Bolli and F. Huang, "Superconducting filter for radio astronomy using interdigitated, capacitively loaded spirals," *Exp. Astron.*, vol. 33, no. 1, pp. 225–236, Mar. 2012.
[17] F. Perini, "Low noise design experience for the SKADS/BEST demonstrator," in *Proc. Final Conf. Wide Field Astron. Technol. Square Kilometre Array (SKADS)*, Ottignies, Belgium, Nov. 2009, pp. 341–345.
[18] G. Valente, A. Navarrini, and T. Pisanu, "Double ridged 180° hybrid power divider with integrated band pass filter," *IEEE Microw. Wireless Compon. Lett.*, vol. 21, no. 1, pp. 13–15, Jan. 2011.
[19] G. Valente, G. Montisci, and S. Mariotti, "High-performance microstrip directional coupler for radio-astronomical receivers at cryogenic temperature," *Electron. Lett.*, vol. 50, no. 6, pp. 449–451, Mar. 2014.
[20] J. D. Gallego and M. W. Pospieszalski, "Design and performance of cryogenically-coolable ultra low noise, L-band amplifier," Nat. Radio Astron. Observatory, Charlottesville, WV, USA, Electron. Division Internal Rep. 286. [Online]. Available: https://www.gb.nrao.edu/electronics/edir/edir286.pdf
[21] Brooks Automation. *Multiple Uses of Model 22C/350C Cryodyne Refrigerators*. Accessed: Dec. 31, 2021. [Online]. Available: http://www.astrosen.unam.mx/Ens/Instrumentacion/manuales/cid/cryogenics.pdf
[22] J. G. Weisend II, *Handbook of Cryogenic Engineering*, 1st ed. New York, NY, USA: Taylor & Francis, 1998.
[23] W. M. Rohsenow, J. R. Hartnett, and Y. I. Cho, *Handbook of Heat Transfer*, 3rd ed. New York, NY, USA: McGraw-Hill, 1998.
[24] *NIST Cryogenics Technologies Group*. Accessed: Dec. 31, 2021. [Online]. Available: https://trc.nist.gov/cryogenics/materials/materialproperties.htm
[25] S. Weinreb, "Cryogenic performance of microwave terminations, attenuators, absorbers, and coaxial cable," Nat. Radio Astron. Observatory, Charlottesville, WV, USA, Electron. Division Internal Rep. 223, Jan. 1982. [Online]. Available: https://www.gb.nrao.edu/electronics/edir/edir223.pdf
[26] J. D. Kraus, *Radio Astronomy*. New York, NY, USA: McGraw-Hill, 1966.
[27] D. M. Pozar, *Microwave Engineering*. Hoboken, NJ, USA: Wiley, 2012.
[28] R. Schwarz. *The Y Factor Technique for Noise Figure Measurements*. Application Note, Accessed: Dec. 31, 2021. [Online]. Available: https://scdn.rohde-schwarz.com/ur/pws/dl_downloads/dl_application/application_notes/1ma178/1MA178_4e_NoiseFigure.pdf
[29] A. Ericsson, D. Sjoberg, G. Gerini, C. Cappellin, F. Jensen, P. Balling, N. J. G. Fonseca, and P. de Maagt, "A contoured-beam reflector satellite antenna using two doubly curved circular polarization selective surfaces," *IEEE Trans. Antennas Propag.*, vol. 69, no. 2, pp. 658–671, Feb. 2021.
[30] R. Cicchetti, V. Cicchetti, A. Faraone, L. Foged, and O. Testa, "A compact high-gain wideband lens vivaldi antenna for wireless communications and through-the-wall imaging," *IEEE Trans. Antennas Propag.*, vol. 69, no. 6, pp. 3177–3192, Jun. 2021.
[31] K. Lu, K. W. Leung, and N. Yang, "3-D-printed circularly polarized twisted-ridge horn antenna," *IEEE Trans. Antennas Propag.*, vol. 69, no. 3, pp. 1746–1750, Mar. 2021.

GIUSEPPE VALENTE received the M.S. degree in electronic engineering and the Ph.D. degree in electronic engineering and computer science from the University of Cagliari, Cagliari, Italy, in 2007 and 2016, respectively. From 2009 to 2016, he was with the National Institute for Astrophysics (INAF), Cagliari Astronomy Observatory, Cagliari, where he worked on the development of the receivers for the Sardinia Radio Telescope. Since 2016, he has been a Researcher at Italian Space Agency and he is currently a Project Scientist of Sardinia Deep Space Antenna and RF Systems. His research interests include electromagnetic design for deep-space applications, in particular low noise microwave systems and radiofrequency calibration instrumentation.

TONINO PISANU received the M.S. degree in physics from the University of Cagliari, Cagliari, Italy, in 1995. Since 2001, he has been a Technologist at the National Institute for Astrophysics (INAF), Cagliari Astronomy Observatory, Cagliari. His research interests include analysis and design of microwave components for radio-astronomy applications and in research and development of non-contact measuring systems for characterizing and correcting the optical shape and mechanical configuration of big antenna systems.

ALESSANDRO NAVARRINI received the S.M. degree in physics from the University of Florence, Florence, Italy, in 1996, and the Ph.D. degree in electronics and microelectronics from the Université Joseph Fourier, Saint Martin d'Hères, France, in 2002. He was with the Institut de Radioastronomie Millimétrique (IRAM), France, from 1998 to 2003, where he worked on the development of low-noise superconductor-insulator-superconductor receivers for the Atacama Large Millimeter Array (ALMA) and the IRAM Observatories. From 2003 to 2006, he was a Postdoctoral Fellow with the Radio Astronomy Laboratory, University of California, Berkeley, CA, USA, where he contributed to the development of the Combined Array for Research in Millimeter-Wave Astronomy (CARMA) Observatory. In 2006, he joined the National Institute for Astrophysics (INAF), Astronomical Observatory of Cagliari, Italy, to work on the instrumentation for the 64-m diameter Sardinia Radio Telescope (SRT). In parallel with his research commitment, he held a teaching position at the Universities of Cagliari. From 2010 to 2015, he was in charge of the Front-End Group at IRAM, that developed the new receivers for the Northern Extended Millimeter Array (NOEMA), France, and the IRAM 30-m diameter radio telescope at Pico Veleta, Spain. In 2015, he returned to the INAF-Astronomical Observatory of Cagliari, where he currently carries out research in low-noise microwave and millimeter-wave radio astronomy receivers, including multi beams and phased array feeds (PAF). He is the National Coordinator of the PAF activities at INAF in the framework of the Square Kilometer Array (SKA) Observatory Development Program (ODP). He is the Executive Director of the contract for the supply of a W-Band Multibeam Receiver for the SRT.

PASQUALINO MARONGIU received the Diploma of D.S.E. degree in industrial engineering (mechanics) from the High School of Sassari, Italy, in 1995. For ten years, he worked in private companies as responsible for mechanical production and quality control. Since 2009, he has been with the National Institute for Astrophysics (INAF), Cagliari Astronomy Observatory, Cagliari, Italy, where he currently works on the development of the receivers and mechanical design for the Sardinia Radio Telescope (SRT).

ALESSANDRO ORFEI received the S.M. degree in electronic engineering from Bologna University, Bologna, Italy, in 1983. He worked for three years at the G. Marconi Foundation Laboratories in the field of the fiber optics and then for three years in a private company as a Design Engineer in the field of telecommunication. Since 1989, he has been a Researcher at the Institute of Radioastronomy (IRA)—National Council for Research, being in charge of all work concerning the very-long-baseline-interferometry (VLBI) 32m antenna at the Medicina Radio Observatory. This same work continued by changing affiliation to IRA—National Institute for Astrophysics, in 2005. He is currently the Head of the Microwave Receiver Group, IRA. His research interests include radio astronomy instrumentation, in particular low-noise microwave receivers, including multi beams and active surface systems for large reflector antennas.

SERGIO MARIOTTI received the High School Diploma in telecommunications, Italy, in 1983. He has been at the Radio Telescope of the Medicina Radio Astronomical Station, Italy, since 1985. He is currently an Experienced Technician with a demonstrated history of working with the National Institute for Astrophysics (INAF). He is skilled in microwave, radio frequency, cryogenics, wire bonding, and test and measurements, such noise figure, network analysis, and phase noise.

RENZO NESTI received the Laurea degree in electronics engineering and the Ph.D. degree in computer science and telecommunications from the University of Firenze, Italy, in 1996 and 2000, respectively. Since December 1999, he has been with the National Institute for Astrophysics, Arcetri Astrophysical Observatory, Firenze, where his main activity is in the area of radio astronomy receivers. His research interests include design and development of microwave passive devices for the receiver front-ends and numerical methods for the electromagnetic analysis and design of millimeter wave components.

JURI RODA received the bachelor's degree in mechanics, in 1992. From 1993 to 1999, he worked in a private company. From 1999 to 2005, he was working at the Istituto di Radioastronomia—Consiglio Nazionale della Ricerche (IRA-CNR). Since 2005, he has been with the Istituto di Radiastronomia—Istituto Nazionale di Astrofisica (IRA-INAF) of Medicina, Bologna, Italy. From 2006 to 2012, he was working on the construction and installation of the SRT 64-m antenna in Sardinia. His work focuses all aspects of structural and mechanical design.

ALESSANDRO CATTANI was born in 1962. He received the bachelor's degree in industrial electronics from ITIS O. Belluzzi, Bologna, Italy, in 1981. Since the year 1983, he has been working with the Institute of Radioastronomy, Medicina Radio Observatory, Italy. Until 1997, he collaborated in the development of equipment for the control and data acquisition of the Northern Cross Radio Telescope, while in the following years, he collaborated in the realization of the JIVE European Correlator and then in the development of receivers for the Sardinia Radio Telescope (SRT). After 1997, he was involved in the development of the prototype instruments for the Low-Frequency Aperture Array for the Square Kilometer Array (SKA) built in Medicina. He is currently working on the control systems of the new receivers for the SRT and for the two 32-m diameter radio telescopes of Medicina and Noto, Italy. Furthermore, he is developing parts of the intermediate frequency (IF) distribution system for the SRT.

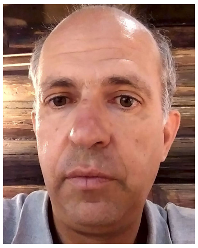

PIETRO BOLLI received the Laurea degree in electronic engineering and the Ph.D. degree in computer science and telecommunications engineering from the University of Florence, Italy, in 1999 and 2003, respectively. In 2002, he started his professional career as a Microwave Engineer at the Italian National Institute for Astrophysics (INAF) conducting research in the field of technology applied to radio astronomy. He is currently a Senior Technologist at the INAF Arcetri Astrophysical Observatory, where he is involved in the design, characterization, and calibration of the low frequency instrument of the Square Kilometer Array. He is the Italian responsible for the protection of the frequency bands used by radio astronomers and represents INAF in the Committee on Radio Astronomy Frequencies (CRAF). He is also an Officer of the Commission J (Radio Astronomy) of the Italian Committee of the Union Radio Scientifique Internationale (URSI). He is the coauthor of about 140 scientific publications, which have appeared in international referred journals and conferences.

GIORGIO MONTISCI (Senior Member, IEEE) received the M.S. degree in electronic engineering and the Ph.D. degree in electronic engineering and computer science from the University of Cagliari, Cagliari, Italy, in 1997 and 2000, respectively. Since November 2015, he has been an Associate Professor of electromagnetic fields at the University of Cagliari, teaching courses in electromagnetics and microwave engineering. He has authored or coauthored more than 70 articles in international journals. His current research interests include the analysis and design of waveguide slot arrays, RFID antennas, wearable antennas, numerical methods in electromagnetics, and microwave circuits and systems. He was awarded the IEEE Access Outstanding Associate Editor of 2020. In 2021, he won a public selection for a Full Professor of electromagnetic fields at the University of Cagliari. He is an Associate Editor of IEEE Access, *IET Microwaves, Antennas and Propagation*, and *Electronics Letters* (IET). He is an Academic Editor of the *International Journal of Antennas and Propagation*.

• • •